ELSEVIER

Journal of Nuclear Materials 289 (2001) 122–127

journal of nuclear materials

www.elsevier.nl/locate/jnucmat

Effects of fission product incorporation on the microstructure of cubic zirconia

L.M. Wang *, S.X. Wang, S. Zhu, R.C. Ewing

Department of Nuclear Engineering and Radiological Sciences, University of Michigan, Ann Arbor, MI 48109-2104, USA

Abstract

Cesium, iodine and strontium ions have been implanted into yttria-stabilized cubic zirconia (YSZ) to determine the effects of fission product incorporation in YSZ that is considered as an inert nuclear fuel matrix. The ion implantation was conducted at room temperature to 1×10^{21} ions/m^2 for each ion with ion energies ranging from 70 to 400 keV. The peak displacement damage level and the peak ion concentration in YSZ reached 205–330 displacement per atoms (dpa) and 11–26 at.%, respectively. The microstructure of the implanted YSZ was studied by in situ and cross-sectional transmission electron microscopy (TEM). In the iodine and strontium implanted samples, a damaged layer with a high density of defect clusters was observed, while in the cesium implanted specimen, most of the damaged layer is amorphous.Nanocrystalline precipitates were observed in the strontium implanted specimen after annealing at 1273 K. The results are discussed in terms of the ionic size, mobility and the solubility of the implanted species in YSZ.

PACS: 28.41.Bm; 61.72.Ff; 61.72.−y; 85.40.Ry

1. Introduction

Yttria-stabilized cubic zirconia (YSZ) is a candidate material for use as an inert fuel matrix for 'burning' excess plutonium in light water nuclear reactors [1–3]. Zirconia is also considered an excellent nuclear waste form for direct geologic disposal [4–6]. Both applications are based on zirconia's high solubility for actinides, excellent chemical durability and exceptional stability under irradiation [1–7]. Because the accumulation of fission and other transmutation products in the zirconia during burn-up may significantly affect the radiation response and the chemical durability of the material, the solubility and mobility of the fission product nuclides in the inert matrix fuel at both high temperature (reactor fuel conditions) and low temperature (repository conditions) are important. Of special interest are the long-lived radionuclides ^{99}Tc, ^{129}I and ^{135}Cs, as well as short-lived ^{90}Sr that can make significant contributions to radiation exposure if released from a nuclear waste repository. There have been only limited studies on the behavior of I [8–11] and Cs [8] in cubic zirconia.

We have utilized ion beam implantation and transmission electron microscopy (TEM) to investigate the solubility of Cs, I and Sr in cubic zirconia, as well as the effects of their incorporation and associated radiation damage on the microstructure. Because ion implantation introduces these ions as extra interstitials with radiation damage, this technique may be used to simulate the effects of fission product incorporation in the zirconia structure, although the ion energies used in this study are much lower than the energies of the fission products formed in the reactor fuel. We have presented preliminary results for Cs-implanted YSZ in a brief report [12], and here we present and compare these results for samples implanted with Cs, I and Sr.

2. Experimental

Well-polished single crystals of a cubic zirconia (1 0 0) wafer (stabilized by 9.5 mol% Y_2O_3) were used as the target material. Ion implantations were first

* Corresponding author. Tel.: +1-734 6478530; fax: +1-734 6478531.

E-mail address: lmwang@umich.edu (L.M. Wang).

0022-3115/01/$ - see front matter
PII: S0022-3115(00)00691-7

conducted using the HVEM/IVEM-Tandem National Facility [13] at Argonne National Laboratory. This allowed the examination by in situ TEM during ion implantation so that the critical ion fluence for any noted effects can be determined. Pre-thinned TEM samples were implanted with 70 keV Cs^+ or 200 keV Sr^+ to 1×10^{21} ions/m^2, respectively, with in situ TEM observation using a 300 keV electron beam. Because the in situ TEM study cannot reveal the depth dependent damage profile, and the thin sample area may contain artifacts due to surface effects, bulk samples were implanted at either the Michigan Ion Beam Laboratory or Argonne National Laboratory using 200 keV I^+, 400 keV Cs^+ and Sr^+ also to 1×10^{21} ions/m^2 for cross-sectional TEM examination. All implantations were conducted at room temperature. Cross-sectional samples were prepared using a 'wedge' technique as described in detail by Zhang [14] with limited Ar ion milling using a Gatan Precision Ion Polishing System (PIPS). The dose rate used for the implantations was 4×10^{16} ions/m^{2}s, and the monitored temperature rise due to beam heating was <50 K.

The depth distribution of implanted ions and displacement damage for the implantations has been simulated by detailed Monte Carlo calculations using the Stopping and Range of Ions in Matter (SRIM) 2000 code [15], which is the newly upgraded version of the TRIM code. The displacement energy of YSZ was assumed to be 40 eV [7] for the purpose of the calculations. The results of the calculations for 400 keV Cs and 200 keV I implantations are shown in Fig. 1. The implantations resulted in peak ion concentration in the range of 11–26 at.% for the three ions and peak displacement damage levels in the range of 205–330 displacement per atoms (dpa). The calculated range of damage were 175, 250 and 110 nm for 400 keV Cs, 400 keV Sr and 200 keV I, respectively.

The Sr implanted bulk sample was annealed at 1273 K for 2 h to study the effect of temperature and increased Sr mobility on the microstructure. This sample was studied by cross-sectional TEM after annealing.

3. Results

In situ TEM during the 70 keV Cs^+ implantation revealed a high density of defect clusters on the nanometer scale after $\sim 2 \times 10^{20}$ Cs/m^2. The defect clusters, with characteristics of interstitial type dislocation loops, are interpreted to be the result of planar precipitates of Zr and/or O interstitials displaced from their original lattice site by the collisional events [12]. The formation of dislocation loops indicates a high defect mobility in YSZ at the room temperature, and this is consistent with previous results of radiation studies that amorphization does not occur even at a dose of 680 dpa [7]. However, amorphous domains in the thin regions of the specimen were observed after 1×10^{21} Cs/m^2 with ex situ high resolution TEM (HRTEM) and nanobeam electron diffraction in areas with a Cs concentration of 11 at.%, as measured by energy dispersive X-ray spectroscopy (EDS) [12]. Because the 70 keV implanted Cs ions were only present in a thin layer of $\sim$30 nm at the surface and the ion distribution is sharply depth dependent, only the average Cs concentration through the entire thickness can be obtained from the planar-view TEM sample. Cross-sectional TEM of the 400 keV Cs-implanted specimen (Fig. 2) confirmed the formation of an amorphous layer that is approximately centered at the depth of peak Cs-concentration, rather than the peak-damage depth. The nature of the amorphous layer was confirmed by both HRTEM and convergent beam electron diffraction (Fig. 3). The top and lower boundaries of the amorphous band correspond to a Cs-concentration of

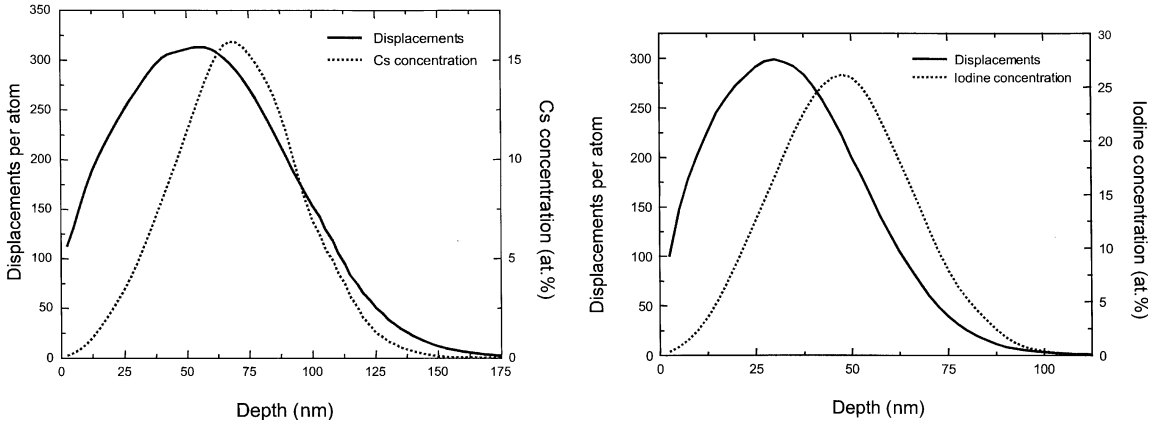

Fig. 1. Depth profile of displacement damage and implanted ion concentration in YSZ calculated by SRIM 2000 with an E_d of 40 eV: (a) 400 keV Cs to 1×10^{21} ions/m^2; (b) 200 keV I to 1×10^{21} ions/m^2.

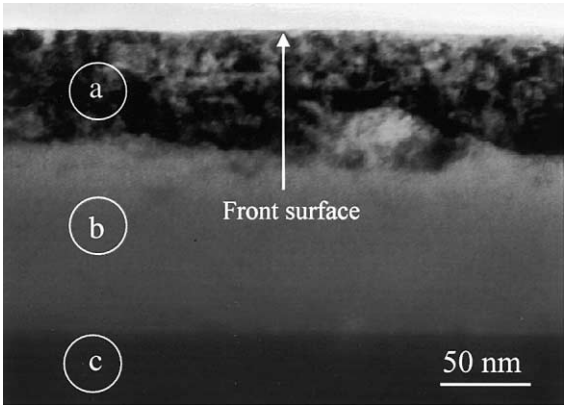

Fig. 2. Bright-field cross-sectional TEM micrograph showing the depth dependent microstructure of YSZ after 400 keV Cs implantation to 1×10^{21} ions/m^2 at room temperature.

$\sim$8 at.% [12]. Strain contrast in the TEM image at the top of the amorphous layer indicates the formation of a high density of defect clusters and local lattice distortion.

The results of the 200 keV I^+ implantation on the microstructure of YSZ are shown by the bright- and dark-field TEM images in Fig. 4. A band ($\sim$50 nm wide) of defect clusters was apparent towards the end of the calculated ion and damage range, but no amorphization was observed throughout the thickness even at depths with $\sim$26 at.% I or $\sim$200 dpa. Although a more detailed study of the damaged band revealed some Moiré fringes

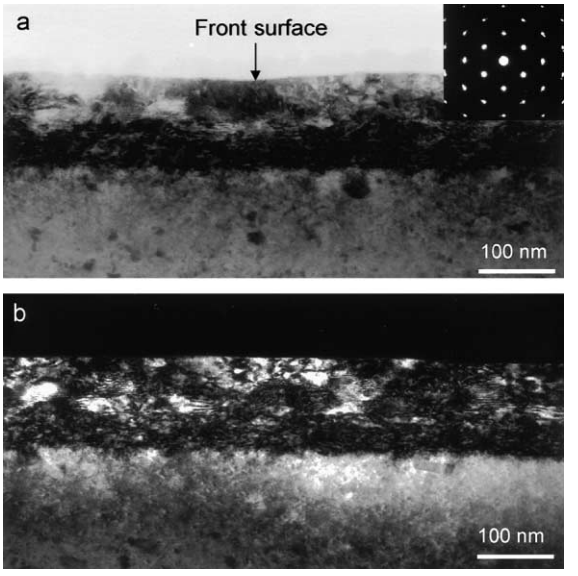

Fig. 4. Bright-field (a) and dark-field (b) cross-sectional TEM micrographs of a YSZ single crystal after a 200 keV I^+ implantation to 1×10^{21} ions/m^2 at room temperature. The selected area electron diffraction pattern in (a) shows that the damaged layer remained a single crystal.

that may be indications of the formation of precipitate phases, the selected area electron diffraction pattern from the damage band showed that the area is still a single crystal (insert of Fig. 4(a)). The defect clusters may include dislocation loops (two-dimensional point

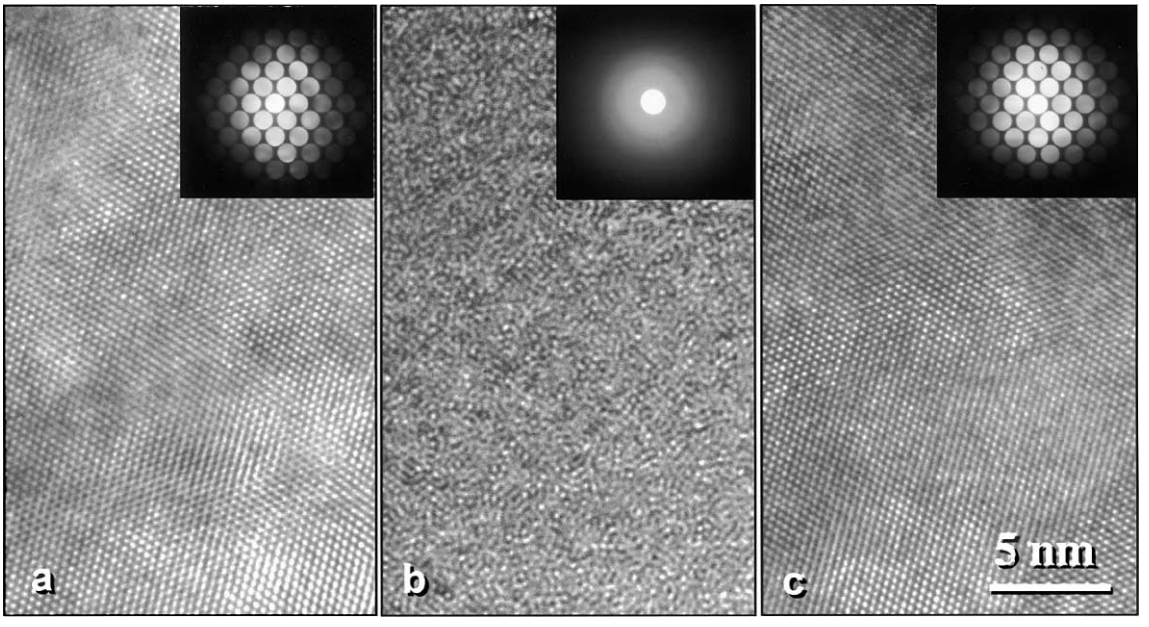

Fig. 3. High resolution TEM micrographs with corresponding convergent electron diffraction patterns from the areas marked as (a), (b) and (c), respectively.

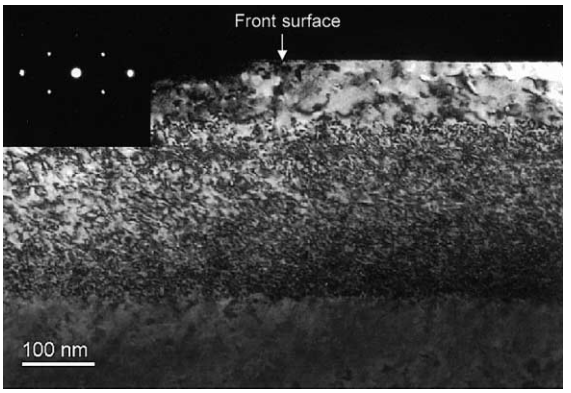

Fig. 5. Dark-field cross-sectional TEM micrograph ($g = 220$) and selected area electron diffraction pattern of a YSZ single crystal after 400 keV Sr^+ implantation to 1×10^{21} ions/m^2 at room temperature showing the depth dependent damage structure.

defect clusters), as well as small three-dimensional precipitates of interstitials. Because of the high concentration of implanted iodine in the region, most of these defect clusters probably contain iodine.

In situ TEM during the 400 keV Sr^+ implantation also revealed a high density of defect clusters on the nanometer scale after $\sim 2 \times 10^{20}$ ions/m^2, but no evidence of amorphization or secondary phase precipitation after 1×10^{21} ions/m^2. The results were confirmed by cross-sectional TEM after 400 keV Sr^+ implantation to 1×10^{21} ions/m^2 as shown in a dark-field image ($g = 220$) of Fig. 5. The defect clusters appear to be dislocation loops with diameters ranging from 3 to 20 nm. The depth of the damage distribution is 50 nm deeper than the calculated damage range and occurs closer to the implanted ion concentration maximum, rather than the displacement damage maximum, which may be due to the high interstitial concentration at the peak ion concentration. Annealing of the Sr-implanted sample at 1273 K for 2 h did not remove the dislocation loops from the damaged microstructure. When the strain field for dislocation loops was tilted out of contrast, small precipitates and cavities were observed in the damaged band. Because the depth at which the precipitates form corresponds to the depth of the maximum concentration of implanted Sr, the precipitates were assumed to contain Sr. A more detailed analysis of the nature and orientation of these nano-scale precipitates is underway, and the results will be presented elsewhere [16].

4. Discussion

Previous irradiation studies have demonstrated that cubic zirconia is one of the most radiation-resistant ceramics [7,17–23]. Naguib and Kelly [24] have classified zirconia as an oxide that is among the most resistant to irradiation-induced amorphization based on its high bonding ionicity. Swelling in cubic zirconia, without excess gas implantation during neutron irradiations, is minimal although prismatic dislocation loops can be easily generated. Stabilized cubic zirconia can also be destabilized to the monoclinic structure under ionizing irradiation [17]. Recently, irradiation to doses as high as 680 dpa [7] and with an implanted xenon concentration as high as 37 at.%, have failed to amorphize cubic zirconia. The observation of dislocation loops at cryogenic temperatures and the readily formed xenon bubbles confirm the high mobility of point defects and implanted xenon atoms in zirconia. This high mobility promotes defect recombination and precipitation, and this prevents the build-up of defects or impurity concentrations required for solid-state amorphization. The recently reported radiation-induced polygonization of cubic zirconia at 120 K [25] is consistent with the structure's strong tendency to crystallize, as polygonization is a result of the competition between radiation-induced amorphization and radiation-enhanced crystallization that is usually observed just above the critical amorphization temperature [26]. Our observation of radiation-induced dislocation loops in the ion-implanted YSZ is consistent with previous observations [2,7].

Although cubic zirconia is known to have high solubility for actinides, there are only limited data on the solubility and mobility of Cs, I and Sr in cubic zirconia. Pouchon et al. [27] recently estimated by thermodynamic calculations that the solubility of Cs_2ZrO_3 (at 1000 K) and Cs (at 2000 K) in ZrO_2 may only be 1.5 at.%, although the highly defective zirconia structure may incorporate higher concentrations of impurities because the impurities may be trapped at the boundaries of crystal defects. The relatively low solubility of Cs in cubic zirconia suggests that Cs tends to precipitate in the secondary phases. The precipitation of a secondary phase is prevented by the extremely low Cs-mobility in cubic zirconia at temperatures below 873 K [9]. Apparently, the amorphization of YSZ implanted with excess Cs is related to the low solubility and mobility of Cs in YSZ.

The effects of implanted impurities on amorphization have been previously noted in several materials. Zinkle and Snead observed that implantation of certain chemical species, such as Si, has a significant effect on amorphization threshold dose for many ceramic materials [28] including alumina (Al_2O_3), magnesium aluminate spinel ($MgAl_2O_4$), magnesia (MgO), silicon nitride (Si_3N_4) and silicon carbide (SiC). For example, the amorphization of Si_3N_4 by a 2 MeV Si ion irradiation is primarily controlled by the Si-concentration, rather than the displacement damage level (i.e., amorphization did not occur in regions well-separated from the implanted

ions for doses up to at least 3 dpa at 80 K); whereas, amorphization did occur at the depths where the implanted Si- concentration was >100 appm for damage levels as low as 0.6 dpa [29]. Similarly, Li et al. [30] reported an amorphous layer in Xe-implanted rutile (TiO_2) that coincided with the measured maximum of Xe-concentration, rather than with the maximum displacement damage.

An important parameter in determining the effect of the implanted species on the threshold amorphization dose is the relative atomic size. The atomic size ratio in crystalline materials has been used to estimate phase stability. As an example, the atomic size ratio (R_A/R_B) determines the occurrence of hydrogen-induced amorphization in the AB_2-type cubic Laves phase system, for which compounds with a ratio >1.37 are amorphized by hydrogenation [31].

Cubic zirconia has the fluorite structure in which zirconium is 8-coordinated by oxygen and oxygen is 4-coordinated by zirconium. To maintain the fluorite structure, the radius ratio of cation to anion should typically be in the range of 0.732–1. In pure zirconia, the ratio is 0.79 (radius of $Zr^{4+} = 0.098$ nm in 8-fold coordination). Zr^{4+} may be substituted by larger cations. However, the maximum cation radius is 0.124 nm, which is approximately that of O^{2-}. Cs^+ is a large cation with an effective ionic or crystal radius ranging from 0.174 or 0.188 (8-coordinated) to 0.188 or 0.202 nm (12-coordinated) [32]. In comparison, the effective ionic radii of Sr and I (as cations) have ranges up to 0.140 and 0.109 nm, respectively, and the effective ionic and crystal radii of xenon ranges from 0.04 to 0.062 nm. Thus, Cs^+ is incompatible in the cubic zirconia structure. The incorporation of Cs^+ or cations with ionic radii larger than 0.124 nm disrupts the local topology in cubic zirconia, which leads to amorphization of the structure at high ion fluences. The monovalent charge of Cs^+ is also incompatible with the fluorite structure. Cs^+ may try to react with O_2^- to form Cs_2O, which has the inverse fluorite structure (i.e., with Cs ions occupying the 4-coordinated anion positions and O occupying the 8-coordinated cation positions in YSZ). For such a reaction, a large amount of local atomic rearrangement has to be made.

The ionic radii of I^- is large (0.22 nm), however, it is unlikely that implanted I^+ will be present in the zirconia as an anion. As cations, iodine radii are much smaller than that of Cs. According to the measurement of I^+ implanted YSZ by Rutherford Backscattering (RBS), iodine diffusion in YSZ is limited below 1373 K [11] indicating a high iodine retention capacity and a rather low iodine mobility in YSZ at lower temperatures. Although the formation of Sr-containing precipitates in the Sr-implanted specimen after annealing suggested a relatively low Sr-solubility at the room temperature in the YSZ matrix, excess Sr (because of the relatively small ionic size) did not cause amorphization of YSZ.

Because the operating temperature of an inert matrix-fuel in nuclear reactors will be quite high (ranging from >1600 K at the core to 873 K at the rim) [3], Cs-migration, release and precipitation are expected. It is unlikely that the Cs-concentration will be greater than 8 at.% in the fuel. Thus, zirconia used as an inert matrix fuel will not become amorphous due to in-reactor irradiation. Nevertheless, our results show that if excess Cs is generated and retained in the YSZ structure at lower temperatures, amorphization may occur. Amorphization can cause a significant increase in the leach rate of a nuclear waste form [33].

5. Summary

Room temperature implantations of I^+ and Sr^+ into YSZ to concentrations up to 26 and 11 at.%, respectively, with displacement damage levels up to 300 dpa induced defect clusters in YSZ, but did not cause amorphization. After annealing of the Sr-implanted sample at 1273 K for 2 h, Sr- containing nanocrystals, as well as voids, precipitated; however, the dislocation loops remained in the microstructure. YSZ was amorphized after a Cs^+-ion implantation of 1×10^{21} ions/m^2 at room temperature with Cs-concentration of 8–16 at.% and displacement damage levels up to 330 dpa. Amorphization of YSZ is caused by the large size incompatibility and the low mobility of Cs ions in the cubic zirconia structure at the room temperature.

Acknowledgements

The authors thank L.L. Funk and the HVEM/IVEM-Tandem Facility at the Argonne National Laboratory for providing the Cs^+ and Sr^+ beams, V.H. Rotberg and the Michigan Ion Beam Laboratory for providing the I^+ beam. Electron microscopy was completed, in part, at the Electron Microbeam Analysis Laboratory at the University of Michigan. This work is supported by US Department of Energy under grant DE-FG07-99ID13767.

References

[1] K.E. Sickafus et al., Ceram. Bull. 78 (1999) 69.
[2] C. Degueldre, J.-M. Paratte, Nucl. Tech. 123 (1998) 21.
[3] V.M. Oversby, C.C. McPheeters, C. Degueldre, J.M. Paratte, J. Nucl. Mater. 245 (1997) 17.
[4] R.B. Heimann, T.T. Vandergraaf, J. Mater. Sci. Lett. 7 (1988) 583.
[5] W.L. Gong, W. Lutze, R.C. Ewing, J. Nucl. Mater. 277 (2000) 239.

[6] G.R. Lumpkin, J. Nucl. Mater 274 (1999) 206.
[7] K.E. Sickafus, H. Matzke, T. Hartmann, K. Yasuda, J.A. Valdez, P. Chodak III, M. Nastasi, R.A. Verrall, J. Nucl. Mater. 274 (1999) 66.
[8] C. Degueldre, M. Pouchon, M. Doebli, G. Ledergerber, in: S.J. Zinkle et al. (Eds.), Microstructural Processes in Irradiated Materials, Mater. Res. Soc. Symp. Proc., vol. 540, Pittsburgh, PA, 1999, p. 337.
[9] N. Chevarier, F. Brossard, A. Chevarier, D. Crusset, N. Monocoffre, Nucl. Instrum. and Meth. B 141 (1998) 487.
[10] K.E. Sickafus et al., Nucl. Instrum. and Meth. B 141 (1998) 358.
[11] M.A. Pouchon, M.M. Döbeli, C. Degueldre, Nucl. Instrum. and Meth. B 148 (1999) 783.
[12] L.M. Wang, S.X. Wang, R.C. Ewing, Philos. Mag. Lett. 80 (2000) 341.
[13] C.W. Allen, E.A. Ryan, Microscopy Res. Tech. 42 (1998) 255.
[14] H. Zhang, Thin Solid Films 320 (1998) 77.
[15] J.F. Ziegler, The Stopping and Range of Ions in Matter (http://www.research.ibm.com/ionbeams/SRIM), IBM-Research, York Town, NY, 1999.
[16] L.M. Wang, S. Zhu, S.X. Wang, to be published.
[17] M.M.A. Sekkina, T.M.A. El-Halim, Thermochim. Acta 113 (1987) 185.
[18] B. Baufeld, D. Baither, U. Messerschmidt, M. Bartsch, I. Merkel, J. Am. Ceram. Soc. 76 (1993) 3163.
[19] H. Inui, H. Mori, H. Futita, Acta. Metall. 37 (1989) 1337.
[20] M.C. Wittels, J.O. Stiegler, F.A. Sherrill, React. Sci. Technol. 16 (1962) 237.
[21] E.L. Fleischer, J. Mater. Res. 9 (1991) 1905.
[22] N. Yu, K. Sickafus, P. Kodali, M. Nastasi, J. Nucl. Mater. 244 (1997) 266.
[23] N. Sasajima, T. Matsui, K. Hojou, S. Furuno, H. Otsu, K. Izui, T. Muromura, Nucl. Instrum. and Meth. B 141 (1998) 487.
[24] H.M. Naguib, R. Kelly, Radiat. Eff. 25 (1) (1975) 1.
[25] J.A. Valdez, C.J. Wetteland, T. Hartmann, A.P. Schreve, R.B. Dyer, S.R. Foltyn, K.E. Sickafus, Nucl. Instrum. and Meth., in press.
[26] L.M. Wang, S.X. Wang, R.C. Ewing, A. Meldrum, R.C. Birtcher, P. Newcomer Provencio, W.J. Weber, Hj. Matzke, Mater. Sci. Eng. A 286 (2000) 72.
[27] M.A. Pouchon, M. Döbeli, C. Degueldre, M. Burghartz, J. Nucl. Mater. 274 (2999) 61.
[28] S.J. Zinkle, L.L. Snead, Nucl. Instrum. and Meth. B 116 (1996) 92.
[29] S.J. Zinkle, L.L. Snead, W.S. Eatherly, J.W. Jones, D.K. Hensley, in: S.J. Zinkle et al. (Eds.), Microstructural Processes in Irradiated Materials, Mater Res. Soc. Symp. Proc., vol. 540, Pittsburgh, PA, 1999, p. 305.
[30] F. Li, P. Lu, K.E. Sickafus, C.R. Evans, M. Nastasi, in: S.J. Zinkle et al. (Eds.), Microstructural Processes in Irradiated Materials, Mater. Res. Soc. Symp. Proc., vol. 540, Pittsburgh, PA, 1999, p. 311.
[31] K. Aoki, X.G. Li, T. Masumoto, Acta. Metall. Mater. 40 (1992) 1717.
[32] F.D. Bloss, Crystallography and Crystal Chemistry, Mineralogical Society of America, Washington, DC, 1994.
[33] W.J. Weber et al., J. Mater. Res. 13 (1998) 1434.